Microchimica Acta
https://doi.org/10.1007/s00604-019-3354-4

ORIGINAL PAPER

Simultaneous voltammetric immunodetection of alpha-fetoprotein and glypican-3 using a glassy carbon electrode modified with magnetite-conjugated dendrimers

Priyal Chikhaliwala[1] · Rakesh Rai[2] · Sudeshna Chandra[3]

Received: 18 February 2019 / Accepted: 5 March 2019

Abstract

The authors describe an electrochemical immunoassay for simultaneous determination of alpha-fetoprotein (AFP) and glypican-3 (GPC-3) which are important biomarkers for early detection of hepatocellular carcinoma (HCC). Magnetite (Fe_3O_4) nanoparticles (NPs) were decorated with hyperbranched amino functionalized dendrimers. The modified NPs were coupled to the antibodies against AFP and GPC-3. The electrochemical behaviour of the Fe_3O_4 NPs and dendrimer-modified NPs were studied. A glassy carbon electrode was then modified with the NP-conjugated antibodies and biomolecular interactions were studied by using cyclic voltammetry and electrochemical impedance spectroscopy. Dual differential pulse voltammetric sensing was performed by utilizing the redox probes; Prussian blue for AFP and toluidine blue for GPC-3. The biomarkers can be detected best at voltages of 0.25 mV and – 0.54 mV (vs Ag/AgCl) for AFP and GPC-3, respectively. The low working potentials makes the method more selective over other electroactive species present in real human serum samples. Response is linear in 0.02 to 10 ng mL^{-1} concentration ranges of both AFP and GPC-3; and the respective detection limits are 50 and 70 pg mL^{-1}. The method was validated by analysing spiked human serum samples. In our perception, the method is of great clinical significance as combination of GPC-3 and AFP increases the sensitivity of detection of HCC.

Keywords Biosensor · Simultaneous detection · AFP · GPC-3 · Hepatocellular carcinoma · PAMAM dendrimer · Fe_3O_4 nanoparticles · Cyclic voltammetry · Electrochemical impedance spectroscopy · Differential pulse voltammetry

Introduction

Primary hepatocellular carcinoma (HCC) accounts for 90–95% of liver cancer with increasing mortality rates seen globally over the past few years [1]. Chronic liver damage due to inflammation with hepatitis B and C virus are major risk factors associated with HCC. These factors gradually culminate into liver cirrhosis and mask the symptoms of cancer progression leading to late-stage diagnosis. Diagnostic approaches include imaging techniques such as computerized tomography (CT) scan and magnetic resonance imaging (MRI) along with assessment of tumor marker most commonly being serum alpha-protein (AFP) [2, 3]. For patients with a high risk of developing HCC like patients with cirrhosis, it is not possible to repeat imaging techniques frequently and assessment of serum AFP level in isolation has poor sensitivity and specificity. The techniques used to detect AFP level in blood use enzyme-linked immunosorbent assay (ELISA), radioimmunoassay (RIA), fluorescence, chemiluminescence, mass spectrometric and electrophoretic immunoassays [4–6]. But, these tests require relatively expensive assay kits and sophisticated instruments which makes the method more tedious, time-consuming and labor-intensive. To overcome these challenges, magnetite nanoparticles (Fe_3O_4 NPs) functionalized

Electronic supplementary material The online version of this article (https://doi.org/10.1007/s00604-019-3354-4) contains supplementary material, which is available to authorized users.

✉ Sudeshna Chandra
Sudeshna.Chandra@nmims.edu

[1] SVKM's NMIMS, Sunandan Divatia School of Science, Department of Biological Sciences, Deemed-to-be University, Vile Parle (west), Mumbai 400056, India

[2] Department of HPB and Transplant Surgery, Fortis Hospital, Mulund (west), Mumbai 400078, India

[3] SVKM's NMIMS, Sunandan Divatia School of Science, Department of Chemistry, Deemed-to-be University, Vile Parle (west), Mumbai 400056, India

Published online: 23 March 2019

with first-generation poly-amidoamine dendrimers (G_1; PAMAM) as an electrochemical biosensing platform for early diagnosis of HCC is presented which can simultaneously measure AFP and glypican-3 (GPC-3) from single sample.

Electrochemical biosensor has the ability to be miniaturized and most importantly enables real-time detection of target analytes. Modifying the nanomaterials as synthetic molecular probes onto the electrodes helps to capture the target analytes even in minimum sample volume at low concentrations [7]. The increased surface area of Fe_3O_4 NPs helps enhance electrocatalytic performance and its core enables magnetic separation of target analytes. This makes the assay more sensitive and specific. Dendrimers act as stabilizers and also because of its branched structure offers an excellent platform for binding of biological ligands. PAMAM dendrimers are hydrophilic with highly flexible surface chemistry that can perform multiple electron redox events [8, 9]. The presence of terminal and internal amine groups in the dendrimer makes the overall structure highly polar and electro-conductive in nature. This reactivity is recognized best for low-generation dendrimers since higher generations tend to undergo steric hindrance affecting the customized properties and chemical reactivity of the molecule [10]. Till now, AFP remains clinically approved biomarker for HCC diagnosis. However, its levels are raised even in other types of cancers and benign pathologies of liver [11]. Therefore, glypican-3 (GPC-3) as a novel promising biomarker along with AFP is selected here for biological sensing. GPC-3 expression is found to increase specifically in HCC patients than that in non-cancerous livers [12, 13]. The overall sensitivity of HCC detection can be improved from 50% to 72% by using both the biomarkers simultaneously [14]. For this, bioconjugates (anti-AFP and anti-GPC-3) were covalently linked through glutaraldehyde as cross-linker and each layer casted on electrode was characterized by voltammetric and impedimetric technique. Further, simultaneous detection is demonstrated by differential pulse voltammetry using redox dyes; Prussian blue for AFP and toluidine blue for GPC-3.

Experimental section

Materials and apparatus

Alpha-fetoprotein antibody (anti-AFP) was received from Indian Institute of Science; Bangalore, India as gift sample. Monoclonal glypican-3 antibody (anti-GPC-3), GPC-3 antigen, AFP antigen, anti-goat immunoglobulin (anti-IgG), ferric chloride hexahydrate ($FeCl_3.6H_2O$), ferrous chloride tetrahydrate ($FeCl_2.4H_2O$), human serum albumin (HSA), human AFP and GPC-3 ELISA kits were purchased from Sigma-Aldrich (Mumbai, India, https://www.sigmaaldrich.com/india/company.html). Bovine serum albumin (BSA) was purchased from Sisco Research Laboratories Pvt. Ltd. (Mumbai, India, http://www.srlchem.com). Glutaraldehyde (GA), ammonium hydroxide (NH_4OH, 25%), potassium ferrocyanide [$K_4Fe(CN)_6.3H_2O$] and toluidine blue (TB) were purchased from S. D. Fine Chem Ltd. (Mumbai, India, http://www.sdfine.com/home.aspx). Sodium chloride (NaCl), D-glucose, L-Ascorbic acid (Vitamin C) and hydrochloric acid (HCl) were purchased from Molychem (Mumbai, India, http://www.molychem.net). Uric acid (UA) was purchased from Loba Chemie Pvt. Ltd. (Mumbai, India https://www.lobachemie.com). Potassium chloride (KCl) was procured from Avra Synthesis Pvt. Ltd. (Mumbai, India, http://www.avrasynthesis.com). Disodium hydrogen phosphate anhydrous (Na_2HPO_4) and potassium dihydrogen orthophosphate (KH_2PO_4) were purchased from Thermofischer India Pvt. Ltd. (Mumbai, India, https://www.thermofisher.com/in/en/home.html). The phosphate buffer saline (0.1 M PBS) contained 16 g L^{-1} NaCl, 0.4 g L^{-1} KCl, 2.88 g L^{-1} Na_2HPO_4 and 0.48 g L^{-1} KH_2PO_4. All chemicals were of analytical grade and used as received. Deionized water (D/W) was used to prepare all solutions throughout the experiment. Fourier Transform Infrared spectra (FT-IR) were recorded in the range of 4000–400 cm^{-1} using a Jasco 460 plus model. X-ray diffraction (XRD) measurements were performed using PHILIPS pro analytical powder diffractometer system PW3040/60 at a scan rate of 48°/min ranging 2(θ) from 20° to 80° using Cu K_α radiation producing X-ray with a wavelength of 1.54 Å. The magnetic properties of the samples were determined using Vibrating sample magnetometer (VSM) Lake Shore Model No. 7410, USA up to a field of 2 T at room temperature. Transmission Electron Microscopy (TEM) were performed on JEM-1011 electron microscope under 100 kV accelerating voltage. Zeta potential for all the samples at different pH was investigated using Malvern Nano ZS90 zeta sizer. All electrochemical measurements were conducted on Metrohm Autolab potientostat/galvanostat, PGSTAT204 system controlled by Nova 1.11 software. Electrochemical experiments were performed using a three-electrode cell: Ag/AgCl (KCl saturated) reference electrode, platinum wire as counter electrode and glassy carbon electrode (GCE; 5 mm diameter) as working electrode. Cyclic voltammetry (CV) measurements were recorded in the potential range of −1 to +1 V with a scan rate of 50 mV s^{-1} in 0.1 M PBS pH 7.5 containing 10 mM $K_4Fe(CN)_6$. Simultaneous detection of AFP and GPC-3 in 0.1 M PBS pH 6.5 was carried out by differential pulse voltammetry (DPV) in a potential range of −0.3 to +0.6 V with a scan rate of 10 mV s^{-1} and a pulse amplitude of 25 mV s^{-1}. Electrochemical impedance spectroscopy (EIS) measurements of the modified electrodes were conducted in a frequency range from 0.1 to 100 kHz with an amplitude of sine wave of 10 mV in 0.1 M PBS pH 7.5 containing 10 mM $K_4Fe(CN)_6$.

Synthesis of magnetite nanoparticles modified with the first-generation poly-amidoamine dendrimer (G_1@Fe_3O_4 NPs)

PAMAM dendrimers as redox substrate was previously designed and synthesized [8]. The structure is represented in

Fig.S1 in Electronic Supplementary Material (ESM). It consists of diethylenetriamine as internal core species and five primary amino groups onto its surface. The interior of molecule consist of secondary and tertiary amines making the overall structure redox-active. Iron-oxide (Fe_3O_4 NPs) was surface functionalized by G_1 PAMAM dendrimer using co-precipitation method by modified in-situ process [15]. This section is presented in detail in ESM.

Anti-AFP and anti-GPC-3 immobilization on G_1@Fe_3O_4 NPs

The surface of G_1@Fe_3O_4 NPs which consist of terminal NH_2 groups was targeted for immobilization with antibodies AFP and GPC-3. G_1@Fe_3O_4 NPs (1 mg mL^{-1}) dissolved in D/W were ultrasonicated at room temperature for 30 min. After ultrasonic dispersion, NPs were incubated in 1.5% GA aqueous solution for 60 min. GA activated particles were then washed thrice with 0.1 M PBS buffer. The washing steps were carried out by using an external magnet to concentrate the GA activated G_1@Fe_3O_4 NPs at the bottom. Magnetically separated GA/G_1@Fe_3O_4 NPs were then incubated with 1.5 μg of antibodies (anti-AFP and anti-GPC-3) for 12 h under constant shaking conditions at ambient room temperature. After 12 h, nanobioconjugates was magnetically washed thrice with 0.1 M PBS buffer. Anti-AFP and anti-GPC-3 were immobilized on NPs separately. The surface biofunctionalization of anti-AFP and anti-GPC-3 to G_1@Fe_3O_4 NPs was electrochemically characterized by CV and EIS. Later, these anti-AFP and anti-GPC-3/G_1@Fe_3O_4 NPs were redispersed in 0.1 M PBS buffer and stored at 4 °C until use.

Fabrication of modified GCE

Prior to use, GCE surface was ultrasonically cleaned with ethanol and D/W for 2 mins, respectively. The cleaned electrode surface was drop-casted with G_1@Fe_3O_4 NPs (20 μL, 1 mg mL^{-1}) and air-dried at room temperature. The modified electrode was evaluated at different scan rate (10 to 100 mV s^{-1}). This was done in order to elucidate the process occurring in close proximity to electrode surface. Next, anti-AFP/G_1@Fe_3O_4 and anti-GPC-3/G_1@Fe_3O_4 NPs (20 μL, 1 mg mL^{-1}) were drop-casted on to GCE as affinity bioreceptors for detecting target analytes. Subsequently, GCE was incubated with 10 mg mL^{-1} BSA for 60 min at 37 °C as a protein blocking buffer to prevent non-specific binding of antibody-antigen complex. Between each step, the resulting electrode was rinsed with 0.1 M PBS buffer to remove any physically adsorbed materials. Further, the resulting electrode was incubated with target antigen (AFP and GPC-3; 100 ng mL^{-1}) at 37 °C for 15 min. CV and EIS measurements were performed on two independently prepared electrodes for AFP and GPC-3, respectively.

Simultaneous detection of AFP and GPC-3

For simultaneous detection, two redox dyes; Prussian blue (PB) and TB were immobilized onto anti-AFP and anti-GPC-3, respectively. PB and TB were actively operated as signal tags only to differentiate the detection process of AFP and GPC-3, respectively due to their distinguishable redox potential. PB was formed containing 10 mM $FeCl_3$ and 10 mM $K_4Fe(CN)_6$ adjusted to pH 1.5 with HCl. PB containing anti-AFP/G_1@Fe_3O_4 NPs and TB for anti-GPC-3-G_1@Fe_3O_4 NPs as immunosensing probes were prepared with the same protocol described above for immobilization. In this step, PB and TB dyes were incubated along with respective antibodies under constant shaking for 12 h at room temperature. PB and TB immobilized nanobioconjugates were magnetically washed and re-dispersed in 0.1 M PBS buffer and stored at 4 °C until use.

The fabrication of biosensor for dual detection was carried out on a cleaned electrode surface. At first; PB/anti-AFP/G_1@Fe_3O_4 (10 μL; 1 mg mL^{-1}) and TB/anti-GPC-3-G_1@Fe_3O_4 NPs (10 μL; 1 mg mL^{-1}) was drop-casted together onto GCE and air-dried at room temperature. Then, electrode was incubated with 10 mg mL^{-1} BSA for 60 min at 37 °C to prevent non-specific binding. The resulting electrode was rinsed with 0.1 M PBS buffer to remove any physically adsorbed materials. Further, GCE was subjected to incubation with different concentrations (0.02 to 100 ng mL^{-1}) of AFP and GPC-3 antigens. AFP and GPC-3 antigen-antibody binding complexes at these variable concentrations were simultaneously detected by DPV. Scheme 1 displays the step-wise fabrication of biosensor for AFP and GPC-3 detection.

Real sample analysis

This study was conducted only after the approval from Institutional Ethics Committee (NMIMS/IEC/010/2018). Four healthy human serum samples were collected from hospital and participant informed consent was taken for the same. The samples were collected and tested for normal liver functioning by standard liver function assays viz., serum bilirubin, serum alkaline phosphatase, serum glutamic oxaloacetic transaminase (SGOT) and serum glutamic pyruvic transaminase (SGPT) and prothrombin time. This was done to ensure the normal human serum matrix by excluding the patients with abnormal liver functions. 20 μL of serum sample was spiked with different known concentrations of AFP and GPC-3. The samples were prepared using 0.1 M PBS buffer. GCE was fabricated by the procedure mentioned above and 20 μL of spiked sample was drop-casted as target antigens. The electrode was then incubated at 37 °C for 15 min. Later, it was rinsed with PBS buffer and DPV was measured.

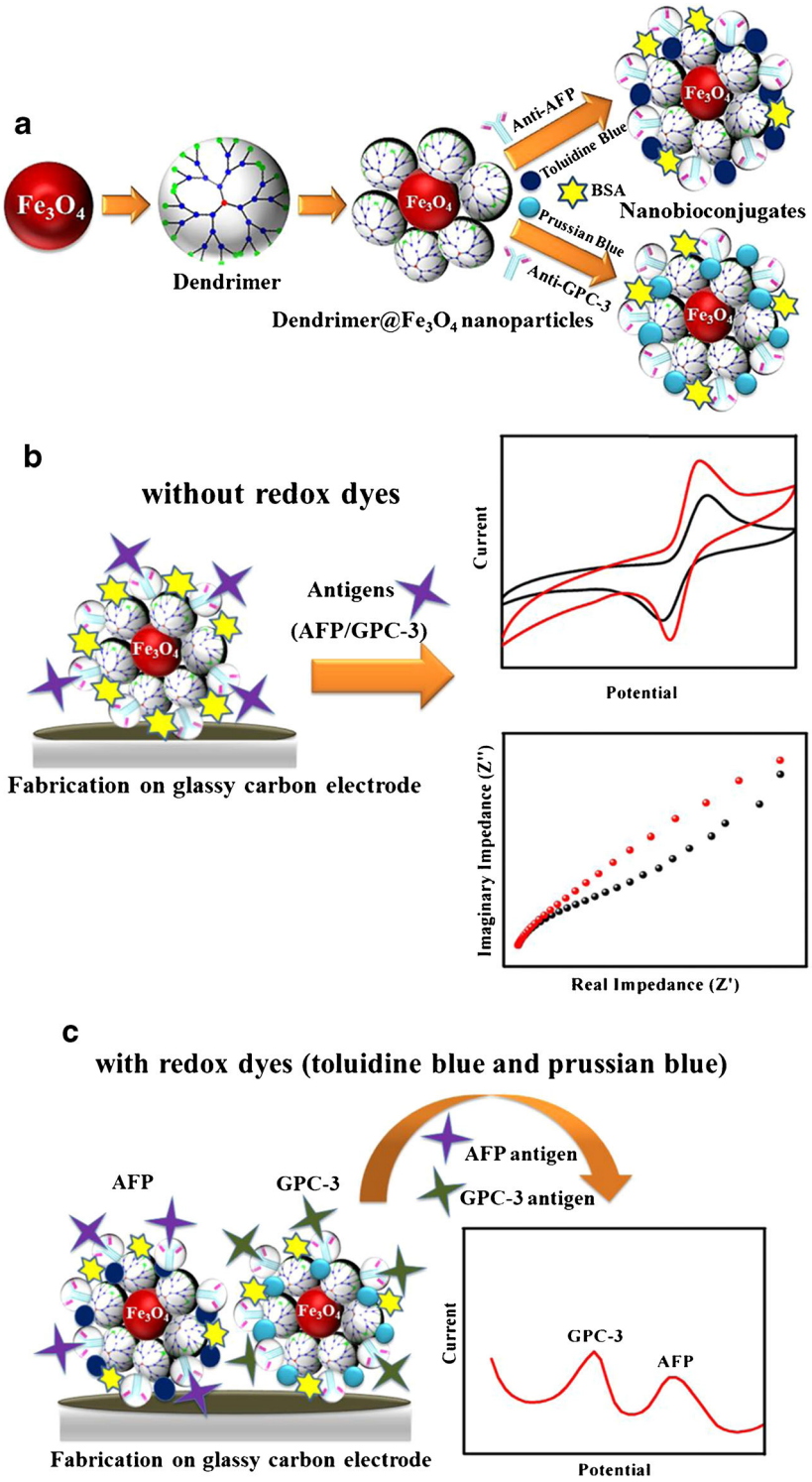

Scheme 1 Schematic representation of step-wise fabrication of biosensor based on PAMAM dendrimer @Fe_3O_4 nanoparticles. **a** Demonstrates synthesis and antibody (anti-AFP and anti-GPC-3) bioconjugation on PAMAM dendrimer@Fe_3O_4 nanoparticles. **b** Fabrication of nanobioconjugates on glassy carbon electrode separately to detect analytes by cyclic voltammetry and electrochemical impedance spectroscopy without using redox dyes. **c** Fabrication of glassy carbon electrode using redox mediator Prussian blue (for AFP) and toluidine blue (for GPC-3) for simultaneous detection of AFP and GPC-3 by differential pulse voltammetry

Results and discussion

Choice of materials

Nanomaterials can be used as electrode materials, since they have large surface area and thus can intensify the loading capacity of biomolecules, thereby improving the sensitivity and detection limit of a biosensor. Among nanomaterials; gold, quantum dots (QDs), carbon nanotubes (CNTs) and reduced graphene oxide (rGO) are intensively studied [16–19]. Colloidal gold NPs (AuNPs) sensing is based on localized surface plasmon resonance (LSPR) transduction. However,

LSPR effect is highly dependent on size, shape, inter-particle distance and dielectric surroundings [16]. Therefore, AuNPs have to be finely tuned according to these variables utilizing different synthesis routes. Also, it involves high cost for large scale production and lack-of-proof towards clinical utility. Much attention is growing towards using zinc oxide (ZnO NPs) [20]. However, when Ni et al. and Fang et al. studied ZnO nanostructures and CNTs modified nanoflowers of ZnO for detection of hydrazine, respectively; the formed sensor resulted in poor detection due to lack of selectivity [21, 22]. Various studies has been reported for QD-antibody bioconjugates in multiplexing. The inherent cross-reactivity of antibodies using color QD multiplex immunoassays still remains a major obstacle in future [23]. CNTs and rGO are also widely used as electrochemical transducer. They are mostly used as electrode scaffolds as they possess good mechanical properties and conductivity. For sensing, CNTs require surface chemical modification as they are commonly insoluble in water. This may sometimes lead to losing partial mechanical strength with harsh chemicals involved and also longer purification steps [24]. Graphene is more versatile as supporting matrix than CNTs; but improving its reproducibility and stability remains a vital challenge [24]. Conducting polymers such as polypyrrole (PPy) and polyaniline (PANI) are also preferred due to ease of immobilization. However, problem of regeneration and distortion of polymeric immobilization matrix still exist [25].

Fe_3O_4 NPs have emerged as promising candidates for sensitive and specific electrochemical transduction as they exhibit strong superparamagnetic property when the size of NP is less than 30 nm [26]. The outstanding advantage using Fe_3O_4 NPs is the possibility to concentrate the target molecules at each modification step by application of external magnet. This is especially useful during immobilization of anti-AFP and anti-GPC-3. The purification process using magnet enhances separation of antibodies conjugated to NPs unlike centrifugation where all the particles settle down. Further, magnetization is also useful during binding of BSA and antigens to modified NPs. Thus, the unbound molecules can be easily separated. So, the conjugates that are attached to NPs can then be drop-casted on electrode and electrochemically measured. This enhances sensitivity and specificity. Also, biological species do not manifest any magnetic behavior and thus, no interferences or noise occurs during signal capturing [27]. As Fe_3O_4 NPs tend to agglomerate easily, dendrimers can act as good stabilizers. Dendrimers with 3D architectures not only provides stability to Fe_3O_4 NPs but also helps in binding various biological ligands to the surface of colloids. PAMAM dendrimers are conductive due to varying polarity of amine groups [8]. They can help enhance redox process as they can undergo protonation in a broad range of pH. At high pH, protonation occurs on the more polar amines, while with lowering of pH, the less polar amines get protonated. With further decrease in pH, the tertiary amines get protonated thereby increasing the internal polarity of the molecule.

Characterization of the G_1@Fe_3O_4 NPs

FTIR spectra of NPs is presented in Fig. S2 in ESM. The spectra shows presence of strong absorption band at 3382, 3422, 3434 and 3434 cm^{-1} for Fe_3O_4, G_1@Fe_3O_4 NPs, G_1 dendrimer and physical mixture. This is because of N–H bond stretch of dendrimer groups. A broad band observed for Fe_3O_4 NPs at 3382 cm^{-1} is due to O–H stretch. Bands observed at 2921 and 2853 cm^{-1} is a result of C–H bond stretch. Band at 1454 cm^{-1} is due to C–H bond bending mode and 1113 cm^{-1} is attributed to C–N bond vibration of dendrimer group. The changes in the intensity of alkyl bond vibration suggest a possible binding interaction of dendrimer carbon group with Fe_3O_4. Band at 1625 cm^{-1} is attributed to the C=O groups in the dendrimer. A characteristic band evident at 580 cm^{-1} for Fe_3O_4 and G_1@Fe_3O_4 NPs is due to symmetric Fe–O bond stretching of metal at tetrahedral site. The physical mixture spectrum differs from G_1@Fe_3O_4 NPs demonstrating favorable binding of G_1 PAMAM dendrimer on to Fe_3O_4 NPs. XRD pattern of G_1@Fe_3O_4 NPs is shown in Fig. S3 in ESM. XRD revealed six diffraction peaks at the crystal plane of (220), (311), (400), (422), (511) and (440) at their corresponding 2θ values of 30.3°, 35.6°, 43.2°, 53.7°, 57° and 62.9°, respectively. The position of analyzed diffraction peaks agree with the XRD of standard Fe_3O_4 pattern reported in literature (ICDD no. 00–019-0629). XRD peaks at the relative positions imply inverse spinel cubic crystal structure. The crystal size D_{XRD} estimated using Scherrer's equation is approximately 4.32 nm which complies with the average particle size determined by TEM (Fig. 1a). The magnetic properties of Fe_3O_4 and G_1@Fe_3O_4 NPs were determined by VSM and is shown in Fig. S4 in ESM. The saturation magnetization (M_s) values were found to be 74 emu g^{-1} and 60 emu g^{-1} for Fe_3O_4 and G_1@Fe_3O_4 NPs, respectively. A certain decrease in M_s Value is recognized for G_1@Fe_3O_4 NPs as account of dendrimer bound to the surface of Fe_3O_4 NPs. VSM magnetization curves for both particles exhibit hysteresis behavior and zero value for coercivity. This indicates that the formed NPs display superparamagnetic behavior. This property was utilized during purification steps by concentrating the biomolecules attached to G_1@Fe_3O_4 NPs using external magnet to increase sensitivity. Details are given in ESM. The structural properties such as size and morphology of G_1@Fe_3O_4 NPs were investigated by TEM and is presented in Fig. 1a, b. TEM micrographs clearly provide evidence of good structural homogeneity, monodispersity and spherical-shaped NPs with negligible aggregation. Figure 1b presents encapsulation of Fe_3O_4 core molecule by organic layers of dendrimer. Mean particle size estimated from histogram is approximately 8.45 ± 2.53 nm. This small-size is attained as a result of stepwise addition of

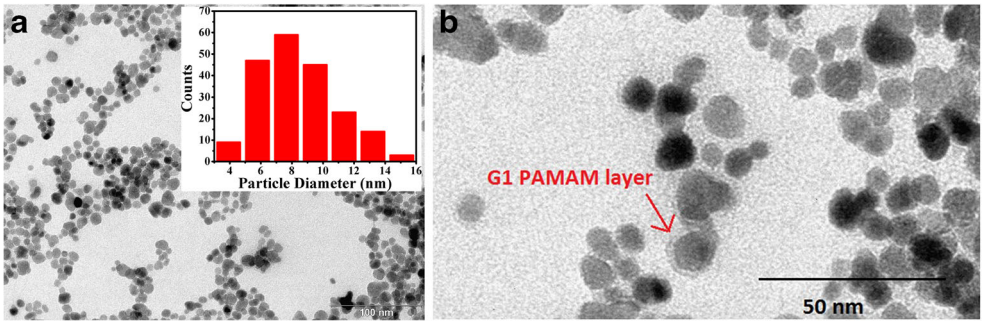

Fig. 1 **a** TEM micrographs of G_1@Fe_3O_4 NPs with monodispersed and spherical-shaped morphology. Inset represents histogram from statistics of 100 NPs. Mean size is approximately 8.45 ± 2.53 nm. **b** Magnified image displaying surface coating of organic layers of PAMAM dendrimer on to Fe_3O_4 NPs

dendrimer at once and appropriate molar ratio of dendrimer to Fe_3O_4, without much affecting the magnetic behaviour (as per VSM results). The selected area electron diffraction (SAED) is shown in Fig. S5 in ESM which displays well-crystallized particles and are in accordance with XRD analysis.

Zeta potential was done to study the surface charge dominated at different pH values of 2, 4, 6, 7, 8, and 10. A plot of G_1@Fe_3O_4 NPs versus pH (2–10) is shown in Fig. 2. At low pH (2–4), a positive surface charge and at higher pH (6–10), negative charge predominates. These findings suggest that at low pH, amine groups of dendrimer undergo protonation acquiring positive charge. It is known that at low pH, tertiary amines are protonated wherein the interior cavity of dendrimer is quite open to promote electrostatic interaction. However, at pH 5.2, the presence of negatively charged stern layer must have neutralized the positive surface. With increase in pH, primary and secondary amines undergo deprotonation interacting with base of alkaline environment and developing negative charge. At physiological pH, NPs tends to achieve good stability. Interestingly, zeta analysis was also performed for antibody and antigen binding to NPs. We note that after antibody conjugation to NP at pH 7, value changes from −16.2 to −19.6 mV and antibody-antigen complex renders value of −20.2 mV. This change is due to the presence of additional amino functionalization of dendrimers and antibody via glutaraldehyde. Since, antigen contains short-chain epitope with characteristic chemical determining group, it implicates a minor change in the surface charge.

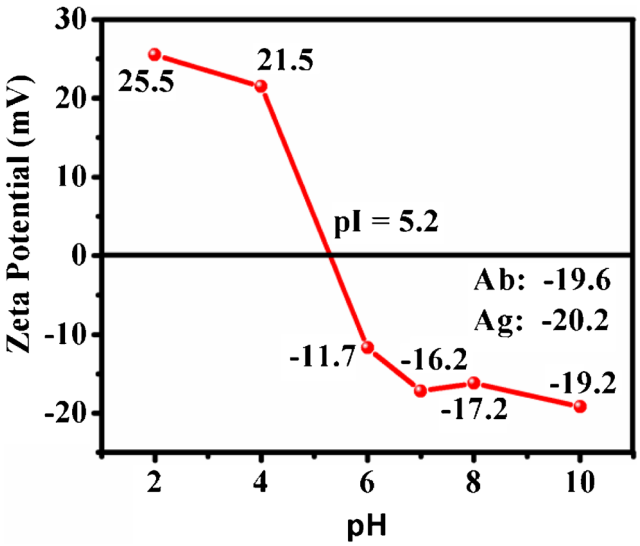

Fig. 2 Graph of zeta potential as a function of different pH from 2 to 10 for G_1@Fe_3O_4 NPs and nano-bioconjugates. Isoelectric point (pI) is at pH 5.2

Electrochemical behavior of the G_1@Fe_3O_4 NPs

Electrochemical behavior of G_1@Fe_3O_4 NPs on GCE was determined by scanning the potential from +1 to −1 V. Different scan rates from 0.01 to 0.2 V s^{-1} was applied to determine the thermodynamic and kinetic process occurring near electrode surface. CVs are displayed in Fig. S6a in ESM. CV analysis revealed linear increase in anodic and cathodic peak current response (I_{pa} and I_{pc}, respectively) with increasing scan rates. This indicates diffusion controlled redox behavior of NPs with an electron-transfer process. Electrochemical parameters such as I_{pa}, I_{pc}, anodic and cathodic peak potential (E_{pa} and E_{pc}, respectively) are displayed in Table S1 and S2 in ESM. Linear plot of I_p versus scan rate is given in Fig. S6b in ESM. Further, the surface concentration of the absorbed electroactive species (G_1@Fe_3O_4 NPs) per unit surface area on GCE was estimated, in accordance with Brown-Anson model and is found to be 1.46×10^{-8} mol cm^{-2}. Also, the diffusion coefficient calculated by Randles-Sevcik equation is 3.90×10^{-4} cm^2 s^{-1}. Details are mentioned in ESM.

Optimization of method

The following parameters were optimized:

(a) Sample pH

pH 6.5 was chosen for simultaneous detection of biomarkers by DPV. Details are given in ESM.

(b) Detection time

The optimum detection time was found to be 15 min. Details are given in ESM.

(c) Concentration of anti-AFP and anti-GPC-3

The optimized concentration for anti-AFP and anti-GPC-3 was 3 μg. The interaction mechanism of antibodies and NPs is represented in Fig. S9 in ESM. Details are given in ESM.

Electrochemical characterization of AFP and GPC-3

CV's for bare GCE, GCE/G_1@Fe_3O_4 NPs, GCE/G_1@Fe_3O_4/Ab, GCE/G_1@Fe_3O_4/Ab/BSA and GCE/G_1@Fe_3O_4/Ab/BSA/Ag is represented in Fig. 3a, b. CV recorded for bare GCE electrode in electrolytic solution of 0 .1M PBS buffer with 10 mM $K_4[Fe(CN)_6]$ functioned as a control measurement to assess electrical changes after each electrode layer assembly. A distinct pair of well-resolved redox peaks is recognized for bare GCE after application of voltage (50 mV s^{-1}). This is due to oxidation and reduction of redox couple $Fe(CN)_6^{4-}$/ $Fe(CN)_6^{3-}$ at electrode/electrolyte interface. When G_1@Fe_3O_4 NP was modified on GCE, it gives rise to sharp increment in peak current. This signal enhancement can be related to polarity of amine groups of dendrimer. The pH of electrolyte solution is approximately 7.5, therefore, the primary and secondary amine groups exposed on the outer shell gets protonated, which is in accordance as per zeta potential results. And, since it's a low generation dendrimer molecule, so $Fe(CN)_6^{3-}$ can easily penetrate through the dendrimer and undergo electron exchange with the underlying electrode. On the other side, approximate 8 nm sized Fe_3O_4 NPs increases the electroactive surface area

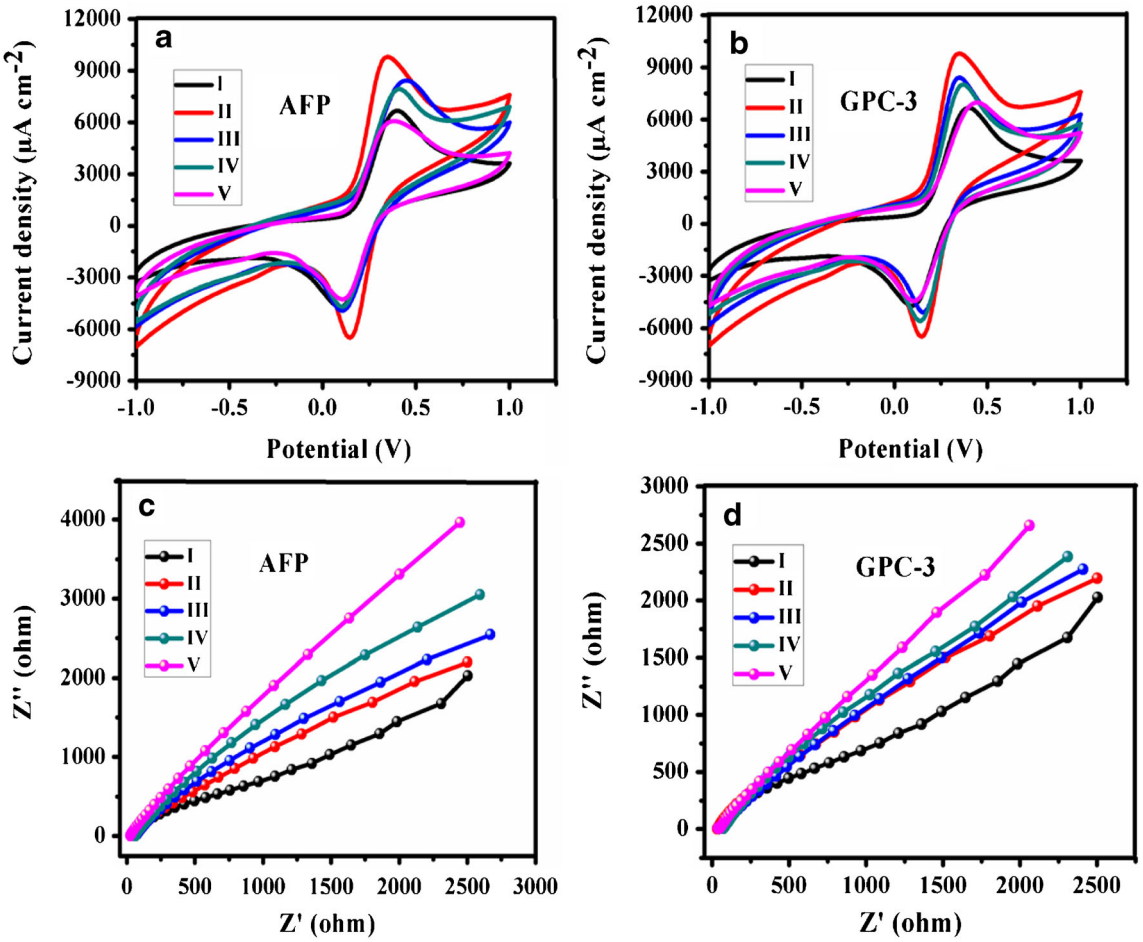

Fig. 3 Electrochemical signal change of CV and EIS during biosensor fabrication process. I. Bare GCE, II. G_1@Fe_3O_4 NPs/GCE, III. Anti-AFP/G_1@Fe_3O_4 NPs/GCE, IV. BSA/anti-AFP/G_1@Fe_3O_4 NPs/GCE, V. AFP/BSA/anti-AFP/G_1@Fe_3O_4 NPs/GCE. **a** CVs for AFP detection. **b** CVs for GPC-3 detection. **c** EIS Nyquist plot acquired for AFP biomarker. **d** EIS Nyquist plot acquired for GPC-3 biomarker. CVs displays decrease in signal current and EIS displays nyquist plot with increasing resistance after each step of biomolecule modification

and exerts its intrinsic electrocatalytic effect facilitating the rate of electron-transfer process and thereby the current signal response. Anti-AFP and anti-GPC-3 immobilization on NP-electrode surface diminishes the current signal, which signifies favorable binding of antibodies to G_1@Fe_3O_4 NPs. Sequentially, when BSA is added to block non-specific sites, the signal further decreases in a similar way. Finally, when corresponding antigens are added, it again lowers the peak current signal. In the detection process, when biological molecules are added stepwise, the current signal declines as a result of increasing layers of non-conductive proteins that bury the electroactive groups of species, thereby, affecting electrode interfacial properties.

For the same approach, a modification step on GCE was also characterized by EIS. EIS technique causes detector to provide detailed insights about the impedance changes occurring on transducer surface due to binding events. Figure 3c, d presents the EIS spectra for each surface modification, best fitted in the form of Nyquist plot. EIS is performed over complete frequency range from 0.1 to 100 kHz. From the impedance response, we analyzed that all Nyquist plots displayed a straight line, which is a characteristic of diffusion-limited electron-transfer process This demonstrates that the nanomaterial exhibits a very low electron-transfer resistance (R_{et}) due to the diffusion of the layer assemblies from the electrode-electrolyte interface. The featured aspect of the impedance process is acquired by fitting the data with model equivalent circuit using ZSimpWin software. The circuit model exhibits resistance in solution (R_s) and polarization resistance (R_p). R_p can occur due to kinetic and diffusion process occurring at electrode and electrolyte interface in which the reactants can move both towards and away from the electrode. It also involves constant phase element (CPE) which occurs because of electrical double layer effect. Importantly, diffusion occurring at low frequency region creates Warburg impedance as a straight line with a slope of 45° as seen in the nyquist plot. The circuit model is provided in Fig. S10 in ESM. R_s and R_p of anti-AFP/G_1@Fe_3O_4 were found to increase from 38.1 Ω and 2.12 kΩ to 71 Ω and 27 kΩ with subsequent deposition of biomolecular layers on electrode surface. Similar trend was observed for anti-GPC-3.

Simultaneous detection and analytical performance of biosensor

G_1@Fe_3O_4 NPs conjugated to anti-AFP and anti-GPC-3 using two redox mediating dyes, as signal tags was used for simultaneously detecting; AFP and GPC-3 biomarkers. Redox dyes; PB (for AFP) and TB (for GPC-3) led to distinguish the analytical signal at different voltages when the NP-antibody modified electrode was exposed to different concentrations of AFP and GPC-3 antigens (0.02, 0.05, 0.1, 0.5, 1, 5, 10, 50, 80 and 100 ng mL^{-1}). DPV current response with increasing concentrations of respective antigens is represented in Fig. 4a. It was noted that the current response decreased gradually with increasing concentrations of biomarkers.

This decrease in current response was observed due to more number of antibody affinity sites occupied by increasing concentration of respective antigens. Thus, when AFP and GPC-3 bind to anti-AFP and anti-GPC-3 modified G_1@Fe_3O_4 NPs electrode, the current response decreases with increasing concentration as there is a formation of more number of immuno-conjugates onto the electrode surface. The antibody-antigen binding with increasing concentrations causes a type of resistance near electrode for charge-transfer to occur. Antibodies and antigens being a protein molecule is electrochemically inactive and therefore this layer on electrode easily blocks electrons to transfer between ferricyanide ions in an electrolyte solution to dendrimer and Fe_3O_4 NPs immobilized on GCE. From the DPV curve, it was seen that AFP and GPC-3 are best detected at working voltages of 0.25 mV and – 0.54 mV (vs Ag/AgCl), respectively. Further, a linear calibration plot with logarithmic concentrations of AFP and GPC-3 in the range from 0.02 to 10 ng mL^{-1} is shown in Fig. 4b, c, respectively. The estimated detection limit of AFP and GPC-3 sensor is 50 and 70 pg mL^{-1} based on three measurements (Signal to noise ratio = 3). The electrochemical sensitivity of the present method for AFP and GPC-3 is 4.61 10^{-4} and 4.86 10^{-4} μA μM^{-1} cm^{-2}, respectively. Thus, the characteristics of Fe_3O_4 NP and PAMAM dendrimer using this strategy led to excellent sensitivity and acceptable LOD values for in practical use. A comparative table on nanomaterial based electrochemical methods for determination of AFP is listed in Table 1. According to this, the present strategy based on immunosensing is far better and comparable to others. To the best of our knowledge, GPC-3 detection is reported here for the first time.

Cross-reactivity, specificity and reproducibility of the immunoassay

It is critical for a diagnosis to evaluate cross-reactivity of analytes to empower the efficiency of process of testing. In a dual detection strategy, there might be chances of cross-reactivity taking place between the two target analytes; AFP and GPC-3 when binding to antibodies. So, to ensure the reliability of sensing process, 0.1 ng mL^{-1} of AFP and GPC-3 binding was checked for cross-reactivity under optimized

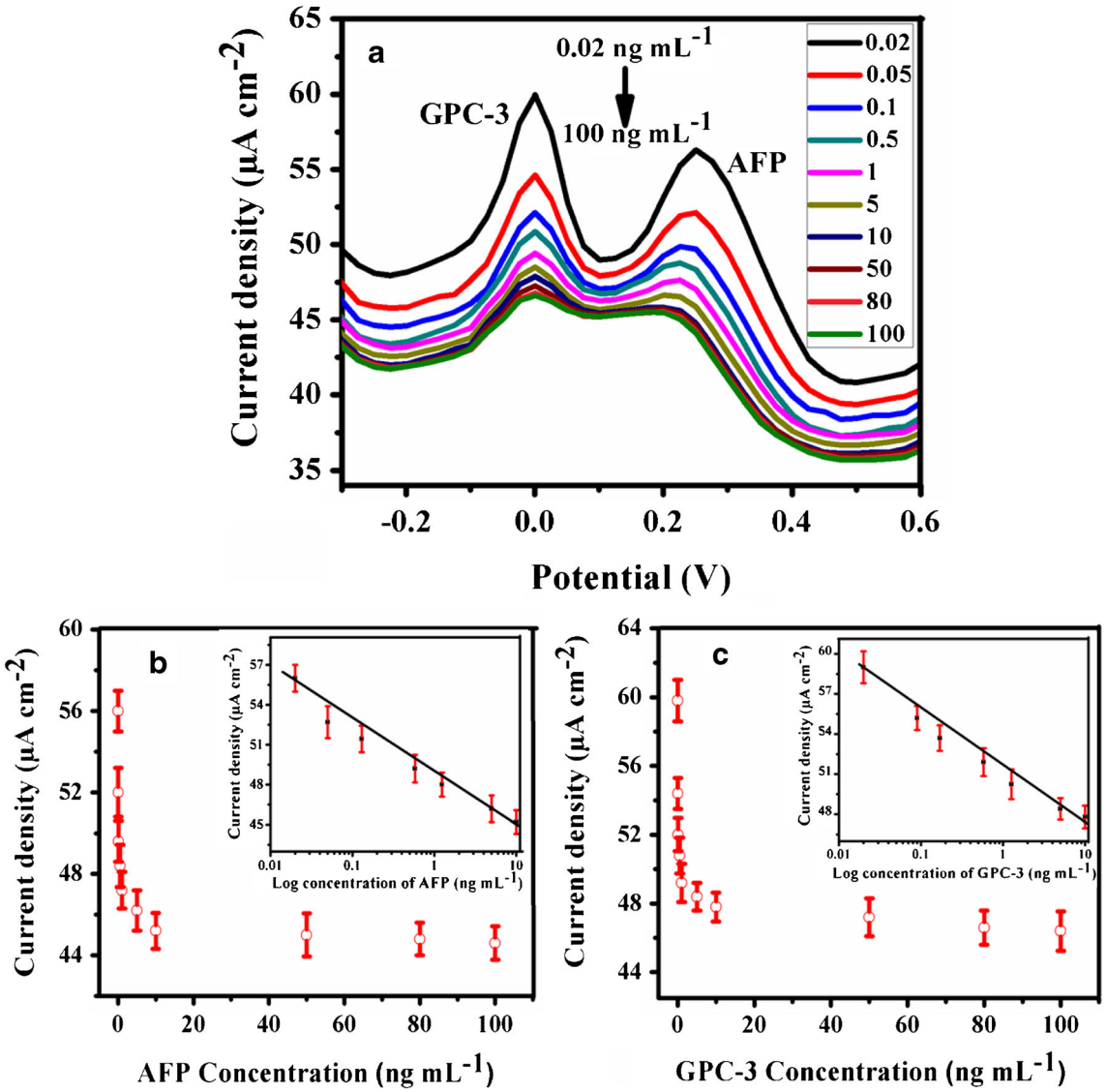

Fig. 4 **a** Simultaneous detection by DPV for AFP and GPC-3 antigens with increasing concentration range from 0.02 to 100 ng mL^{-1}. **b** Standard curve of sensor response plotted for current density versus logarithmic AFP antigen concentration. **c** Standard curve of sensor response plotted for current density response versus logarithmic GPC-3 antigen concentration. Mean ± S.D. ($n = 3$)

Table 1 A comparison of materials and limit of detection (LODs) with other electrochemical methods for the detection of AFP and GPC-3

Materials used	Biomarker	Method	Linear range (ng mL^{-1})	LOD (ng mL^{-1})	Refs.
TH/rGO/AuNPs	AFP	DPV	100-1 10^5	50	[28]
Fe_3O_4/AuNPs/CS/Ab_2	AFP	Amperometry	10–8000	1.78	[29]
Fe_3O_4/AuNPs/Ab_2/MGCE	AFP	Amperometry	20–100	0.64	[30]
Hep/PGA/PPy NPs/GCE	AFP	DPV	0.1–100	0.099	[31]
Fe_3O_4/PL/Hep NPs	AFP	DPV	0.1–100	0.072	[32]
Fe_3O_4/CdTe QDs	AFP	ECL	1–200	0.32	[33]
FeC/AuNPs/MPS/ITO	AFP	DPV	0.5–100	0.1	[34]
Fe_3O_4/PAMAM dendrimer	AFP	DPV	0.02–100	0.05	This work
	GPC-3			0.07	

TH thionine, *rGO* reduced graphene oxide, *AuNPs* gold nanoparticles, *CS* chitosan, *MGCE* magnetic glassy carbon electrode, *Hep* heparin, *PGA* γ-polyglutamic, *PPy* polypyrrole, *PL* ε-polylysine. *CdTe QDs* cadmium telluride quantum dots, *FeC* 6-ferrocenylhexanethiol, *MPS* mesoporous silica, *ITO* indium tin oxide, *ECL* electrochemiluminescence

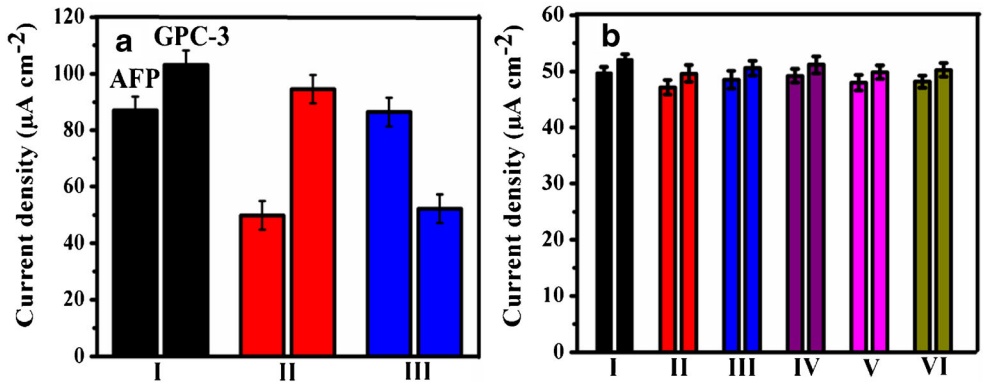

Fig. 5 **a** DPV current response of cross-reactivity of AFP and GPC-3 biomarkers. **I** Control test - AFP and GPC-3 antibody modified NPs, **II** Incubation with 0.1 ng mL^{-1} AFP antigen and **III** Incubation with 0.1 ng mL^{-1} GPC-3 antigen **b** DPV current response of immunosensor to **I** 0.1 ng mL^{-1} AFP and GPC-3, **II** 0.1 ng mL^{-1} AFP and GPC-3 + 10 ng mL^{-1} Glucose **III** 0.1 ng mL^{-1} AFP and GPC-3 + 10 ng mL^{-1} Uric acid **IV** 0.1 ng mL^{-1} AFP and GPC-3 + 10 ng mL^{-1} IgG **V** 0.1 ng mL^{-1} AFP and GPC-3 + 10 ng mL^{-1} HSA **VI** 0.1 ng mL^{-1} AFP and GPC-3 + 10 ng mL^{-1} Ascorbic acid (vitamin C)

conditions. The antibody modified $G_1@Fe_3O_4$ NPs acted as a control measurement and other two DPVs were recorded when AFP and GPC-3 antigens were incubated and assayed separately on the same electrode. The results for cross-reactivity are shown in Fig. 5a. Red column implies current response only in the presence of AFP antigen on same electrode where an obvious decrease in current is observed. However, an insignificant small change in current is also observed for GPC-3. When GPC-3 was incubated (blue column), decrease in current response is reflected. Further, the specificity of immunosensor was confirmed by incubating AFP and GPC-3 antigens (0.1 ng mL^{-1}) with interfering substances normally present in human serum matrix such as 10 ng mL^{-1} glucose, UA, IgG, HSA and ascorbic acid (vitamin C). A negligible change in current response is observed which indicates good selectivity of the immunoassay as seen in Fig. 5b. DPVs of cross-reactivity and specificity are given in Fig. S11 in ESM. To investigate the reproducibility of the immunoassay, 0.1 ng mL^{-1} antigens was electrochemically measured using five independent GCE electrodes. The results are shown in Fig. S12 in ESM and relative standard deviation estimated was 2.97% and 3.38% for AFP and GPC-3, respectively. This indicates acceptable reproducibility. Additionally the storage stability of immunosensor was tested for current response till 30 days and is shown in Fig. S13 in ESM. A negligible change in current response is seen indicating good stability of sensor when stored at 4 °C. Also, the reversibility of the sensor was examined. The electrode was rinsed with 0.1 M HCl to dissociate antigen-antibody complex and regenerate the immunosensor. However, immunosensor binding is rarely reversible and causes a significant loss in the current response. This may be because of the antibody denaturation and loss of activity due to acid wash. Thus, the method is limited in terms of reversibility and sensor can work as single-shot probe.

Application in detection of clinical human serum samples

The analytical reliability of this immunoassay was validated using four human serum samples. The samples collected were checked for normal liver functioning by measuring the levels of liver enzymes; SGOT and SGPT and other standard liver function parameters. Four normal samples were selected and spiked with different known concentrations of AFP and GPC-3 antigens. In this test, 20 μL of spiked serum was added as target analyte onto modified GCE and analyzed using DPV. The peak voltages were displayed at 0.25 mV and – 0.54 mV (vs Ag/AgCl) for AFP and GPC-3, respectively. The current response was plotted against the linear response of the sensor to determine the concentrations of the antigens. The data was compared with the ELISA results as listed in Table 2. Data are means ±SD, *n* =

Table 2 Comparison of the determination values of AFP and GPC-3 in clinical human serum samples

Sample no.	Present method ng mL^{-1}		ELISA method ng mL^{-1}		Relative error %	
	AFP	GPC-3	AFP	GPC-3	AFP	GPC-3
1	7.85	7.81	7.56	8.21	3.83	5.12
2	3.90	3.92	3.95	4.02	−1.26	−2.48
3	1.93	1.95	1.90	1.98	1.57	−1.51
4	0.95	0.97	0.92	1.02	3.26	−4.90

3. A low relative error indicates a good correlation with the data acquired by the reference method. This indicates the feasibility of the biosensor for clinical applications.

Conclusions

An amino-functionalized dendrimer@Fe_3O_4 nanomaterial placed on a GCE electrode was demonstrated as an electrochemical biosensing platform for simultaneous detection of two HCC-specific biomarkers; AFP and GPC-3. Detection of AFP and GPC-3 by CV and EIS signified the electron-transfer process occurring at each steps near electrode interface. This strategy relied on redox-controlled diffusion process between redox couple $[Fe(CN)_6]^{3-/4-}$ and polarity of amine groups of dendrimers. Dendrimers not only enhanced charge-transfer process but also provided large surface area for loading of antibody molecules. On the other hand, Fe_3O_4 nanoparticles facilitated magneto-separation of analytes as well as enhanced the electroanalytical effect in synergy with dendrimers. Dual detection of AFP and GPC-3 by DPV reflected a change in current response. A major limitation resulted from incubation with AFP for cross-reactivity which led to slight decrease of the signal corresponding to GPC-3. Also, immunosensor is not reversible and can be applicable for only single-shot detection. However, the detection limit meets the clinical requirement with threshold value for normal AFP marker being approximately 20 ng mL^{-1}. Thus, it has an immense potential for clinical translation. To our best knowledge, this is the first solid step taken towards simultaneous detection of GPC-3 and AFP in blood sample for early diagnosis of HCC using this technique. Thus, it provides a unique perspective on biomolecule based sensor fabrication and signal output.

Acknowledgments The authors are thankful to Department of Metallurgical Engineering and Materials Science, Indian Institute of Technology Bombay, for XRD and VSM measurements. We acknowledge Dr. Kolja Them (University of Hamburg, Germany) for performing nanoparticle characterization by TEM. Authors are grateful for financial support from Nanomission, Department of Science and Technology [Sanction No.: SR/NM/NB-1024/2016(C)], Government of India for providing research project grant.

Compliance with ethical standards Ethical approval was obtained from Institutional Ethics Committee (NMIMS/IEC/010/2018).

References

1. Yezaz AG, Idrees M, Julie HR (2017) Review of hepatocellular carcinoma: epidemiology, etiology, and carcinogenesis. J Carcinog 16:1–17. https://doi.org/10.4103/jcar.JCar_9_16
2. Schraml C, Kaufmann S, Rempp H, Syha R, Ketelsen D, Notohamiprodjo M, Nikolaou K (2015) Imaging of HCC – current state of the art. Diagnostics 5:513–545. https://doi.org/10.3390/diagnostics5040513
3. Hina AT, Bobby K, Surya C, Puneet S, James C, Rainner WG, Diego RM (2014) MRI of hepatocellular carcinoma: an update of current practices. Diagn Interv Radiol 20:209–221. https://doi.org/10.5152/dir.2014.13370
4. Liu QL, Yan XH, Yin XM, Situ B, Zhou HK, Lin L, Li B, Gan N, Zheng L (2013) Electrochemical enzyme-linked immunosorbent assay (ELISA) for α-fetoprotein based on glucose detection with multienzyme-nanoparticle amplification. Molecules 18:12675–12686. https://doi.org/10.3390/molecules181012675
5. Sallam KM, Sheha R, El-Zahhar AA (2011) Development of solid phase radioimmunoassay system using new polymeric magnetic micro-spheres. J Radioanal Nucl Chem 290:339–345. https://doi.org/10.1007/s10967-011-1188-6
6. Limei A, Feng G, Bifeng P, Rong H, Daxiang C (2006) Fluoroimmunoassay for antigen based on florescence quenching signal of gold nanoparticles. Anal Chem 78:1104–1106. https://doi.org/10.1021/ac051323m
7. Sandeep KV, Venkatesh AG, Konstantinos M, Gregor C, Gunter R, Felix von S, Roland Z (2012) Nanotechnology-based biosensors and diagnostics: technology push versus industrial/healthcare requirements. BioNanoScience 2:115–126. https://doi.org/10.1007/s12668-012-0047-4
8. Sudeshna C, Mumukshu DP, Heinrich L, Dhirendra B (2015) Dendrimer-functionalized magnetic nanoparticles: a new electrode material for electrochemical energy storage devices. J Power Sources 280:217–226. https://doi.org/10.1016/j.jpowsour.2015.01.075
9. Rouhollah K, Gozde U, Serap Y, Gungor G, Ufuk G (2013) PAMAM dendrimer-coated iron oxide nanoparticles: synthesis and characterization of different generations. J Nanopart Res 15:1488–1486. https://doi.org/10.1007/s11051-013-1488-6
10. Vasile E, Serafim A, Petre D, Giol D, Dubruel P, Iovu H, Stancu I (2014) Direct synthesis and morphological characterization of gold-dendrimer nanocomposites prepared using PAMAM succinamic acid dendrimers: preliminary study of the calcification potential. Sci World J 918:1–15. https://doi.org/10.1155/2014/103462
11. Yan-Jie Z, Qiang J, Guan-Cheng L (2013) Tumor markers for hepatocellular carcinoma. Molecular and Clinical Oncology 1:593–598. https://doi.org/10.3892/mco.2013.119
12. Hanlin W, Florencia A, Qihui Z, Brian A, Shang-Tian C, Ximing Y (2008) Glypican-3 as a useful diagnostic marker that distinguishes hepatocellular carcinoma from benign hepatocellular mass lesions. Arch Pathol Lab Med 132:1723–1728. https://doi.org/10.1043/1543-2165-132.11.1723
13. Tangkijvanich P, Chanmee T, Komtong S, Mahachai V, Wisedopas N, Pothacharoen P, Kongtawelert P (2010) Diagnostic role of serum glypican-3 in differentiating hepatocellular carcinoma from non-malignant chronic liver disease and other liver cancers. J Gastroenterol Hepatol 25:129–137. https://doi.org/10.1111/j.1440-1746.2009.05988.x
14. Jiatao L, Lingfei Z, Shaogang LV, Chenzi Z, Shuai J (2017) Biomarkers for hepatocellular carcinoma. Biomark Cancer 9:1–9. https://doi.org/10.1177/1179299X16684640
15. Sascha D, Sudeshna C, Colin G, Senoy T, Denys M, Steffen S, Michael H, Manfred A, Dhirendra B, Heinrich L (2012) Design, characterization and magnetic properties of Fe_3O_4-nanoparticle arrays coated with PEGylated-dendrimers. Mater Chem Phys 132:292–299. https://doi.org/10.1016/j.matchemphys.2011.11.015
16. Milton C, Fabio FC, Pedro P, Antonio L, Pedro VB (2016) Gold nanoparticles for diagnostics: advances towards points of care. Diagnostics 6:1–20. https://doi.org/10.3390/diagnostics6040043
17. Guifen J, Lei W, Jinxin Y, Shusheng Z (2011) Versatile electrochemiluminescence assays for cancer cells based on dendrimer/CdSe-ZnS-quantum dot nanoclusters. Anal Chem 83:3873–3880. https://doi.org/10.1021/ac200383z

18. Joseph W (2005) Carbon-nanotube based electrochemical biosensors: a review. Electroanalysis 17:7–14. https://doi.org/10.1002/elan.200403113
19. Ming Z, Yueming Z, Shaojun D (2009) Electrochemical sensing and biosensing platform based on chemically reduced graphene oxide. Anal Chem 81:5603–5613. https://doi.org/10.1021/ac900136z
20. Ashok KS, Shen-Ming C (2008) Nanostructured zinc oxide particles in chemically modified electrodes for biosensor applications. Anal Lett 41:141–158. https://doi.org/10.1080/00032710701792612
21. Ni Y, Zhu J, Zhang L, Hong J (2010) Hierarchical ZnO micro/nanoarchitectures: hydrothermal preparation, characterization and application in the detection of hydrazine. CrystEngComm 12:2213–2218. https://doi.org/10.1039/b923857n
22. Yu Y, Cuiwen J, Tao L, Jie L, Yegeng F, Yuning W, Feiyan Y, Liping X (2017) A zinc oxide nanoflower-based electrochemical sensor for trace detection of sunset yellow. Sensors 17:1–9. https://doi.org/10.3390/s17030545
23. Kim ES, Thomas P, Igor LM, Hedi M (2006) Biosensing with luminescent semiconductor quantum dots. Sensors 6:925–953. https://doi.org/10.3390/s6080925
24. Cho IH, Lee J, Kim J, Kang MS, Paik JK, Ku S, Cho HM, Irudayaraj J, Kim DH (2018) Current technologies of electrochemical immunosensors: perspective on signal amplification. Sensors 18:1–18. https://doi.org/10.3390/s18010207
25. Almira R, Arunas R (2002) Application of polypyrrole for the creation of immunosensors. Crit Rev Anal Chem 32:245–252. https://doi.org/10.1080/10408340290765542
26. Ling D, Lee N, Hyeon T (2015) Chemical synthesis and assembly of uniformly sized iron oxide nanoparticles for medical applications. Acc Chem Res 48:1276–1285. https://doi.org/10.1021/acs.accounts.5b00038
27. Michael H, Alan LG, Serge C (2014) Nanomaterials for biosensing applications: a review. Frontiers in Chemistry 2:1–10. https://doi.org/10.3389/fchem.2014.00063
28. Li G, Li S, Wang Z, Xue Y, Dong C, Zeng J, Huang Y, Liang J, Zhou Z (2018) Label-free electrochemical aptasensor for detection of alpha-fetoprotein based on AFP-aptamer and thionin/reduced graphene oxide/gold nanoparticles. Anal Biochem 547:37–44. https://doi.org/10.1016/j.ab.2018.02.012
29. Li S, Liang J, Zhou Z, Li G (2018) An electrochemical immunosensor for AFP measurement based on the magnetic Fe_3O_4@au@CS nanomaterials. Mater Sci Eng 382:1–6. https://doi.org/10.1088/1757-899X/382/2/022017
30. Yuan Y, Li S, Xue Y, Liang J, Cui L, Li Q, Zhou S, Huang Y, Li G, Zhao Y (2017) A Fe_3O_4@au-based pseudo-homogeneous electrochemical immunosensor for AFP measurement using AFP antibody-GNPs-HRP as detection probe. Anal Biochem 534:56–63. https://doi.org/10.1016/j.ab.2017.07.015
31. Tingting X, Bo C, Jian G, Meilin C, Wenlu F, Meihui Y, Hong X (2017) Novel electrochemical immune sensor based on Hep-PGA-PPy nanoparticles for detection of α-fetoprotein in whole blood. Analytica Chimica Acta 977:36–43. https://doi.org/10.1016/j.aca.2017.04.045
32. Xu T, Chi B, Wu F, Ma S, Zhan S, Yi M, Xu H, Mao C (2017) A sensitive label-free immunosensor for detection α-fetoprotein in whole blood based on anticoagulating magnetic nanoparticles. Biosens Bioelectron 95:87–93. https://doi.org/10.1016/j.bios.2017.04.015
33. Huang Z-J, Han W-D, Wu Y-H, Hu X-G (2016) Magnetic electrochemiluminescent immunoassay with quantum dots label for highly efficient detection of the tumor marker α-fetoprotein. J Electroanal Chem 785:8–13. https://doi.org/10.1016/j.jelechem.2016.11.060
34. Lin J, Zhang H, Niu S (2015) Simultaneous determination of carcinoembryonic antigen and α-fetoprotein using an ITO immunoelectrode modified with gold nanoparticles and mesoporous silica. Microchim Acta 182:719–726. https://doi.org/10.1007/s00604-014-1378-3